IEEE Access
Multidisciplinary | Rapid Review | Open Access Journal

Received April 9, 2020, accepted April 28, 2020, date of publication May 12, 2020, date of current version May 27, 2020.

Digital Object Identifier 10.1109/ACCESS.2020.2994068

Design of a Twelve-Port MIMO Antenna System for Multi-Mode 4G/5G Smartphone Applications Based on Characteristic Mode Analysis

JIAN DONG[1], SHAN WANG[1], AND JINJUN MO[2]
[1]School of Computer Science and Engineering, Central South University, Changsha 410083, China
[2]School of Information and Communication, Guilin University of Electronic Technology, Guilin 541004, China

Corresponding author: Jinjun Mo (jinjunmo@guet.edu.cn)

This work was supported in part by the National Natural Science Foundation of China under Grant 61801521 and Grant 61971450, in part by the Natural Science Foundation of Hunan Province under Grant 2018JJ2533, and in part by the Fundamental Research Funds for the Central Universities under Grant 2018gczd014 and Grant 20190038020050.

ABSTRACT This paper presents a twelve-port multiple-input multiple-output (MIMO) antenna system for multi-mode 4G/5G smartphone applications. Characteristic mode analysis (CMA) is used to illustrate the operation principle and optimize the geometrical structure of the antenna system. The proposed MIMO antenna system consists of a 4G antenna module and a 5G antenna module. The 4G antenna module is a 2×2 MIMO antenna array capable of covering the LTE700/2500/3400, GSM850/900, DCS, PCS, UTMS, 2.4-GHz WLAN, and 3.5-GHz WiMAX, which consists of two symmetrical antenna elements, and uses protruded ground to improve the isolation between the two adjacent 4G module antenna elements. The 5G antenna module is a 10×10 MIMO antenna array composed of ten identical monopole antennas and operates at the bands of 3.31 $\sim$ 3.70 GHz and 4.46 $\sim$ 5.40 GHz, covering the 3.5-GHz band (3.4 $\sim$ 3.6 GHz) and 4.9-GHz band (4.8 $\sim$ 5.0GHz) for 5G applications. The proposed antenna is fabricated, and the experimental results agree with the simulated results well. The calculated envelope coefficient correlation is lower than 0.5, indicating that the diversity performance meets the need of the MIMO antenna system. All the features make the antenna suitable for multi-mode 4G/5G smartphone applications.

INDEX TERMS MIMO antenna, decoupling, 5G antenna, characteristic mode, smartphone applications.

I. INTRODUCTION

With the development of wireless communications, multi-mode and multi-band antennas are required for mobile phones to incorporate more functions and services and support more communication standards. Additionally, to increase the transmission rate, the multiple-input-multiple-output (MIMO) antenna system is required. It has been demonstrated that MIMO systems with multiple antennas for both the transmitter and receiver can improve the spectrum efficiency and transmission rate of the communication system without increasing the transmission power [1]. However, due to the limited space reserved for smartphone antennas, the design of a multi-band MIMO antenna system with low mutual coupling is a serious technical challenge.

The associate editor coordinating the review of this manuscript and approving it for publication was Raheel M. Hashmi.

In recent years, several decoupling techniques have been proposed to optimize isolation for the MIMO system, such as the neutralization line (NL) technique [2], etching slot method [3], [4], ground branch decoupling method [5]–[7], metamaterial structures [8], and decoupling networks [9]. In [2], a 2×2 MIMO system was proposed for smartphone applications, and its measured S_{21} was lower than -10 dB within the operating bands when adding two crossed neutralization lines. In [3], four slots were etched on the ground to improve the isolation between the antenna elements and this achieved measured S_{21} values lower than -15 dB within the entire band. A decoupled structure composed of lumped elements and three U-shaped slots was proposed in [4], and the measured isolation between two antenna elements was better than 11 dB. In [5], low mutual coupling was obtained over two operating bands by using a folded dual inverted L-shaped ground branch. In [6], the isolation between two antenna elements was improved to 10 dB by using a

decoupled structure of the slotted and protruded ground. A decoupled structure of a fence-shaped ground branch was presented in [7], and the two-element multi-band MIMO antenna system achieved S_{21} values lower than -10 dB within the entire band. A 3-D metamaterial structure in [8] was proposed to reduce the mutual coupling between a two-element MIMO antenna and achieved the isolation higher than 18 dB. A decoupling network composed of a neutralization-line and two phase-shifting lines [9] was added between two antennas to form a decoupled structure. However, the metamaterial structures and decoupling networks were complex and large in size, which means that they are not suitable for smartphone applications.

Meanwhile, the fifth-generation (5G) communication has become a hot spot in the field of mobile communications. Recently, several 5G MIMO antenna designs have been proposed [10]–[15]. In [10], an eight-port MIMO antenna system operating at the 3.5 GHz band was proposed for 5G applications. In [11], an eight-antenna MIMO array was proposed for 5G smartphones, which used a novel balanced open-slot to achieve the band of 3.5 GHz. However, these designs only focused on 3.5 GHz-band of 5G communications, and did not achieve the 5G higher band. In order to realize multi-band operations, eight L-shaped slots based on stepped impedance resonators (SIRs) [12] were used to excite dual-resonance at the LTE band 42 and LTE band 46 for 5G applications. In [13], 10 T-shaped coupled-fed slot antenna elements were used to excite dual resonant modes for 5G smartphone antennas. In [14], an 8×8 MIMO antenna system used four sets of dual-antenna arrays to achieve the dual-band operation of 5G applications. By inducing the coupled-feeding structure in the antenna system [15], two frequency bands, including 3.5 GHz-band and 5 GHz band of 5G applications, were excited. However, the above designs failed to cover the 4G frequency bands simultaneously.

In this paper, a multi-mode MIMO antenna consisting of a 4G antenna module and a 5G antenna module is proposed. The 4G antenna module has two identical antenna elements (2×2 MIMO antenna system) with S_{11} lower than -6 dB over 691-970 MHz, 1430-2740 MHz, and 3360-3960 MHz, covering all the applications of LTE700(698-784 MHz), GSM850(824-894 MHz), GSM900 (880-960 MHz), DCS (1710-1880 MHz), PCS (1850-1990 MHz), UTMS (1920-2170 MHz), LTE2300 (2300-2400 MHz), LTE2500 (2500-2690 MHz), 2.4-GHz WLAN, 3.5-GHz WiMAX (3300-3700 MHz), and LTE3400 (3400-3800 MHz). The 5G antenna module is a ten-antenna array (10×10 MIMO configuration) with S_{11} lower than -6 dB over 3.38 $\sim$ 3.66 GHz and 4.3 $\sim$ 5.18 GHz, covering the 3.5-GHz band (3.4$\sim$3.6 GHz) and 4.9-GHz band (4.8 $\sim$ 5.0 GHz) for 5G applications. In the 4G antenna module, a protruded ground is introduced to improve the isolation between two adjacent 4G antenna elements, which achieves low mutual coupling below -11 dB in the lower band and below -15 dB in the upper bands. In the 5G antenna module, the isolation between each pair of adjacent

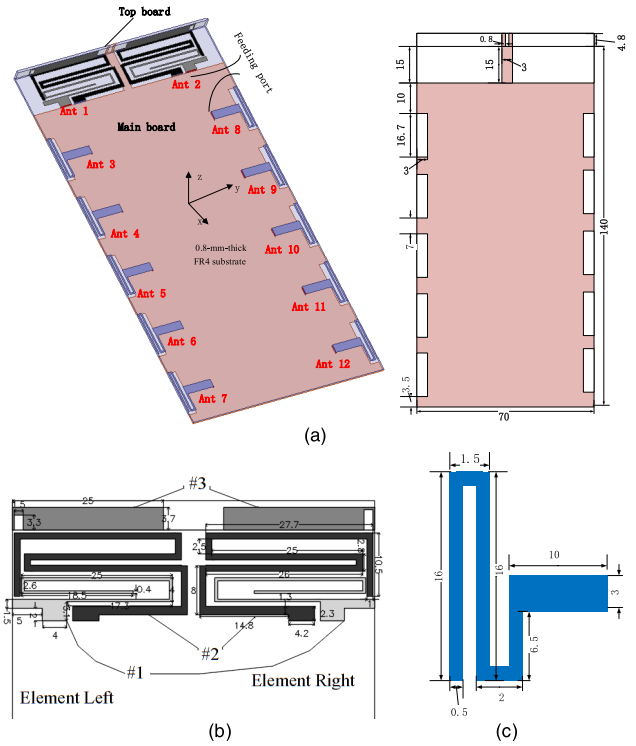

FIGURE 1. Geometry and detailed dimensions (in millimeters) of the proposed antenna system: (a) general view; (b) detailed dimensions of the 4G antenna module structures; (c) detailed dimensions of the 5G antenna module structure.

elements is higher than 12.5 dB in the lower band and 15 dB in the upper band because of the enough distance between them. Furthermore, characteristic mode analysis (CMA) is introduced to illustrate the operation principle and optimize the geometrical structure of the 4G and 5G antenna module. In the following sections, we will first describe the antenna configuration and its operating principle, and then present the simulated and measured results to validate the performance of the proposed antenna system.

II. ANTENNA CONFIGURATION

Fig. 1 presents the geometrical configuration and detailed dimensions of the proposed twelve-port MIMO antenna system. The twelve-port MIMO antenna system is printed on a main board and a top board, as shown in Fig. 1(a). Both boards are fabricated by an FR4 substrate ($\varepsilon_r = 4.4$, $tan\delta = 0.02$), and the dimensions of them are $140 \times 70 \times 0.8$ mm^3 and $4.8 \times 70 \times 0.8$ mm^3, respectively. It is suitable for a typical 5.5- inch smartphone. The 4G module consisting of two identical antennas (Ant 1 and Ant 2) is printed at the top edge of the proposed antenna system. The 5G module consisting of ten identical antennas (Ant 3 to Ant 12) is printed along two long side edges. As shown in Fig. 1(b), the 4G module includes two symmetric antenna elements. Each element is composed of two bending structures in the main board (#1 and #2) and a rectangular patch with a small rectangular slot in the top board (#3). The structures #1, #2 and #3 are responsible for the excitation of low

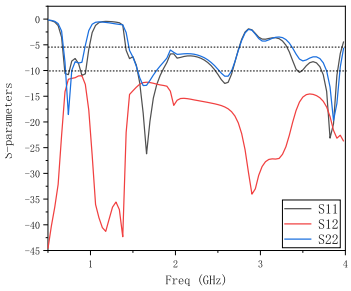

FIGURE 2. Simulated S-parameters of Ant 1 and Ant 2.

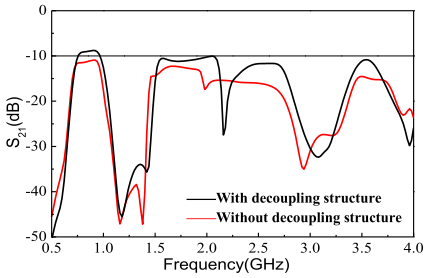

FIGURE 3. Simulated S-parameters of the proposed antenna with and without decoupling structure.

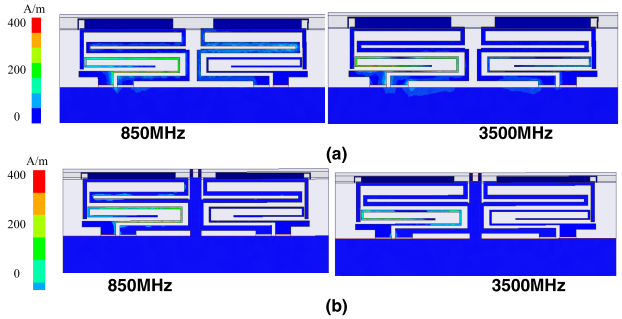

FIGURE 4. Simulated surface current distributions of the proposed 4G antenna module system at different frequencies: (a) without decoupling structure, (b) with decoupling structure.

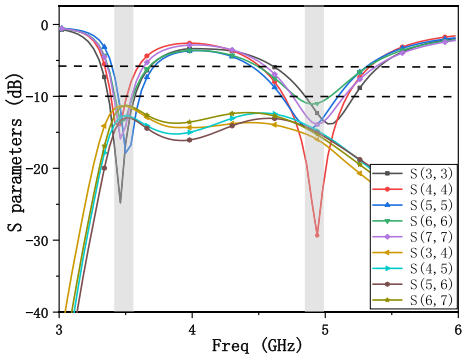

FIGURE 5. Simulated S-parameters of Ant 3 to Ant 7.

frequency band, medium frequency band, and high frequency band, respectively. Fig. 1(c) shows the detailed dimensions of the 5G module antenna module structure. Fig. 1(a) shows that the decoupling structure consists of a rectangular protruded ground in the ground plane of the main board and two rectangular protruded grounds in the back of the top board to improve the isolation for the 4G antenna system. Each feeding structure is connected to a 50 Ω coaxial cable. Ten rectangular clearance regions of 16mm × 3mm are etched in the ground for the 5G antennas.

The 4G antenna module has two identical antenna elements (2 × 2 MIMO antenna system) with S_{11} lower than −6 dB over 691-970 MHz, 1430-2740 MHz, and 3360-3960 MHz, covering all the applications of LTE700(698-784 MHz), GSM850(824-894 MHz), GSM900 (880-960 MHz), DCS (1710-1880 MHz), PCS (1850-1990 MHz), UTMS (1920-2170 MHz), LTE2300 (2300-2400 MHz), LTE2500 (2500-2690 MHz), 2.4-GHz WLAN, 3.5-GHz WiMAX (3300-3700 MHz), and LTE3400 (3400-3800 MHz). The simulated S-parameters of 4G module antennas are presented in Fig. 2. As shown in Fig. 2, the mutual coupling between two antennas is below −11 dB in the lower band and below −15 dB in the upper bands.

The decoupling structure consists of a rectangular protruded ground in the ground plane of the main board and two rectangular protruded ground in the back of the top board, and achieves S_{21} values below −11 dB within the operating bands. Fig. 3 shows the simulated S-parameters of the proposed antenna with and without the decoupling structure. The mutual coupling is obviously reduced in all bands, especially in the low frequency section. To explain the importance of the decoupling structure, Fig. 4 presents the simulated surface current distribution on the 4G antenna module at 850 MHz and 3400 MHz. In both cases, the Ant1 is excited and the Ant2 is terminated by a matching load. From the comparison of Fig. 4 (a) and Fig. 4 (b), it is observed that the current flowing to Ant 2 is significantly reduced after introducing the decoupling structure to the 4G antenna module.

The 5G antenna module consisting of ten identical antennas (Ant 3 to Ant 12) are printed on the two long side edges of the main board, as shown in Fig. 1(a). The simulated S-parameters of the 5G module's five left hand side antennas are presented in Fig. 5. Owing to the symmetry of the antennas on two sides with respect to the central line of the system circuit board, the results of Ant8 to Ant12 are generally identical to those of Ant3 to Ant7. For brevity, Fig. 5 only presents the results of Ant3 to Ant7. As can be seen in this figure, the simulated reflection coefficients (S_{33}, S_{44}, S_{55}, S_{66}, and S_{77}) of five antennas are less than −6 dB (3:1 VSWR) in the bands of 3.31 ∼ 3.70 GHz and 4.46 ∼ 5.40 GHz, covering the 3.5-GHz band and 4.9-GHz band for 5G applications. The isolation between each pair of adjacent elements is higher than 12.5 dB in the lower band and 15 dB in the upper band because of the enough distance between them.

III. OPERATING PRINCIPLE BASED ON CHARACTERISTIC MODE ANALYSIS

A. CMA OF 4G ANTENNA MODULE

Characteristic mode analysis (CMA) is a useful method for finding potential resonance and explaining the operating prin-

ciple of the antenna physically. By the definition of CMA, the characteristic modes of an antenna are only affected by its shape and material, and are irrelevant to excitation.

Characteristic modes can be defined by

$$X\left(J_{s,n}\right) = \lambda_n R\left(J_{s,n}\right), \tag{1}$$

where λ_n is the characteristic eigenvalue and $J_{s,n}$ is the eigenvector; X and R are the imaginary and real part of the impedance matrix, respectively. The mode will be considered to be a resonant mode when λ_n is equal to 0.

The modal significance (MS) illustrates the ability of each characteristic mode coupling with an external source. It is independent of the external source and is an inherent property of the characteristic modes. It can be described in the following equation:

$$MS = |\frac{1}{1 + j\lambda_n}|. \tag{2}$$

The mode is a significant mode which can be excited when $MS \geq \frac{1}{\sqrt{2}}$.

In order to illustrate the operating property of the proposed 4G antenna module, the characteristic mode analysis of 4G antennas with different configurations is presented respectively. Fig. 6 shows the geometries of various antennas involved in the design evolution process and the modal significance of Antenna (1) is presented in Fig. 7. As shown in Fig. 7, Antenna (1), which consists of structure #1 (as shown in Fig. 1(b)), has two significant modes. If properly excited, Antenna (1) can resonant at 0.8 GHz (mode 1) and 2.5 GHz (mode 2).

As can be observed from (3), the total current distribution of a mode, J_s, is determined by the modal significance and the external excitation V_n^{ex}. Therefore, the positions and ways of feeding are crucial to the generation of characteristic modes

$$J_s = \sum\nolimits_n \frac{V_n^{ex} J_{s,n}}{1 + j\lambda_n} \tag{3}$$

Fig. 8 presents the characteristic current distributions of mode 1 and mode 2 at their resonant frequencies. As shown in Fig.8, when Antenna (1) works at mode 1, most of the current is concentrated on structure #1. When Antenna (1) works at mode 2, most of the current is concentrated on the ground. As can be seen by equation (3), the feeding position is very important to the total current distribution. Since we do not feed the ground, mode 2 cannot be excited. Therefore, Antenna (1) resonates at 0.8 GHz after feeding structure #1.

In order to obtain a higher effective frequency band, structure #2 is added to the 4G antenna system (see Antenna (2)). Fig. 9 presents the CMA of Antenna (2). As shown in Fig. 9(a), four new modes (mode 2 to 5) emerge by adding structure #2. Fig. 9 (b) presents the characteristic current distributions of these modes. We can see that these new modes are brought about by structure #2 from Fig. 9 (b). The resonant frequencies of mode 2 to mode 5 are 1.5 GHz, 3.3 GHz, 2.5 GHz and 4 GHz, respectively. The resonances corresponding to mode 1-5 are excited after feeding the

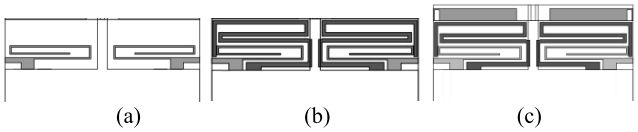

FIGURE 6. Geometries of various antennas involved in the design evolution process: (a) Antenna (1), (b) Antenna (2), (c) Antenna (3).

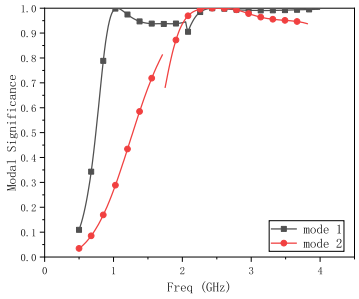

FIGURE 7. Modal significance of Antenna (1).

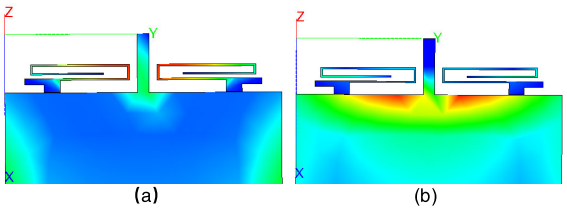

FIGURE 8. Characteristic current distributions of Antenna (1): (a) mode 1 at 0.8GHz, (b) mode 2 at 2.5GHz.

antenna. However, the impedance matching of high frequency band which is brought about by mode 4 and 5 is too bad to be used for WiMAX and LTE3400 applications.

In order to obtain the frequency band of WiMAX and LTE3400 applications, structure #3 is added to the 4G antenna system. It can be observed from Fig. 10 that a new mode which resonates at 3.3 GHz emerges and the modal significance of mode 6 (mode 5 in Antenna (2)) is enhanced by adding structure #3. Therefore, Antenna (3) could better resonate at 3.3 GHz and 4 GHz, covering the frequency band of WiMAX and LTE3400 applications.

Fig.11 presents the simulated return loss of antennas with different configurations It is evident from this figure that the low frequency band (0.6-0.9 GHz) is mainly excited by adding structure #1. The blue curve in Fig. 11 clearly shows that the addition of structure #2 (see Antenna (2)) brings about a high frequency band (1.5-2.8 GHz). The higher frequency band (3.3-3.9 GHz) is mainly excited by adding structure #3. In order to obtain a higher effective frequency band for WiMAX and LTE3400 applications, two rectangular slots are etched on structure #3 (see Antenna (3)).

B. CMA OF 5G ANTENNA MODULE

In order to explain the operation property of the proposed 5G antenna module, characteristic mode analysis (CMA) of the 5G antenna module was performed. Fig. 12 presents the

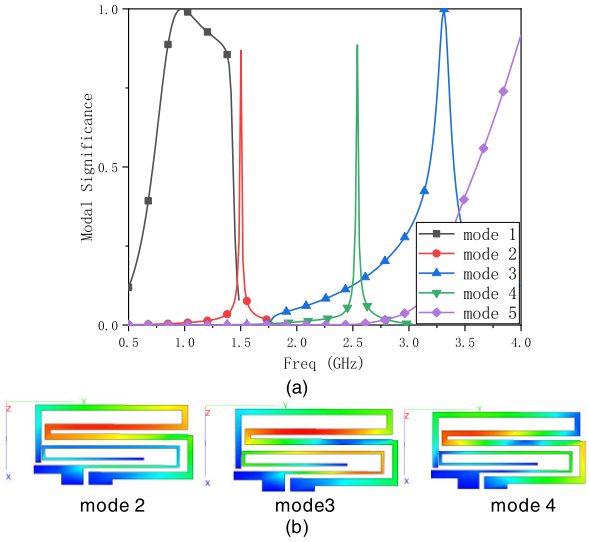

FIGURE 9. Characteristic mode analysis of Antenna (2): (a) Modal significance of Antenna (2), (b) Characteristic current distributions of Antenna (2).

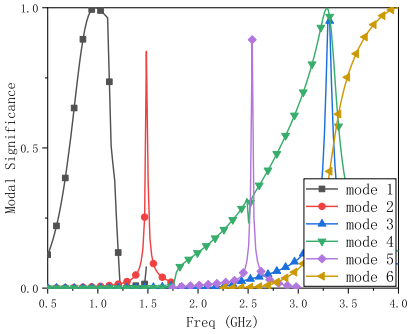

FIGURE 10. Modal significance of Antenna (3).

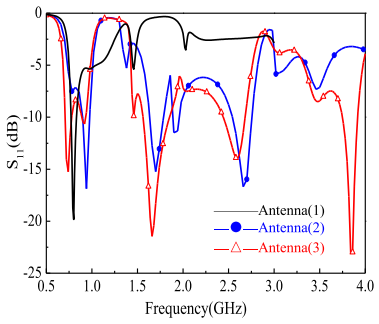

FIGURE 11. Simulated return loss for various antenna geometries.

modal significance of the first five modes for the proposed 5G module antenna. It can be seen from Fig. 12 that the 5G module antenna has two effective modes in the required frequency bands. The resonant frequency of mode 1 is 4.9 GHz and the resonant frequency of mode 2 is 3.4 GHz. Fig. 13 presents the characteristic current distributions of mode 1 and mode 2 at their resonant frequencies. As shown in Fig. 13, most of

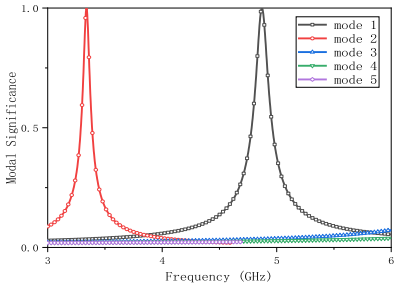

FIGURE 12. Modal significance of the first five modes for the proposed 5G module antenna.

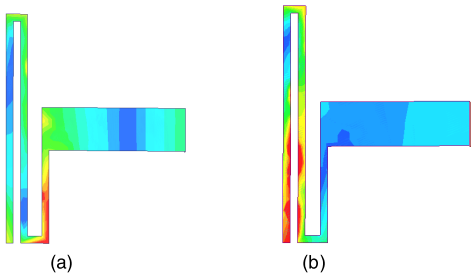

FIGURE 13. The characteristic current distributions of the proposed 5G module antenna: (a) mode 1 at 4.9GHz, (b) mode 2 at 3.4GHz.

the currents are concentrated on the shortest branch and the medium branch at mode 1 and most of the currents are concentrated on the longest branch and the medium branch at mode 2. Therefore, the characteristic mode 1 is produced by the shortest branch and the medium branch, and the characteristic mode 2 is produced by the longest branch and the medium branch.

In order to obtain the optimal structure of the 5G module antenna, a parametric study was performed based on the above results of characteristic mode analysis. We adjusted the frequency band of mode 1 (band II-4.9 GHz) by changing the length of the shortest branch (L3) and the medium branch (L2), and adjusted the frequency band of mode 2 (band I-3.5 GHz) by changing the length of the longest branch (L1) and the medium branch (L2). When one parameter is tuned, all the other parameters are fixed. Fig. 14 presents the S-parameters of Ant 3 in the 5G module with different values of (a)L1, (b)L2, and (c)L3. As shown in Fig. 14, the resonant frequency of band I shifted to a lower frequency when L1 increased, while the resonant frequency of band II remained essentially unchanged. The resonant frequency of band I and the resonant frequency of band II shifted toward a lower frequency at the same time when L2 increased. The resonant frequency of band II shifted toward a lower frequency, while the resonant frequency of band I remained essentially unchanged when L2 increased. In order to cover both band I and band II, the values of L1 = 16 mm, L2 = 16.5 mm and L3 = 6.5 mm are chosen as optimums. Therefore, band I is mainly excited by the longest branch and the medium branch and band II is excited mainly

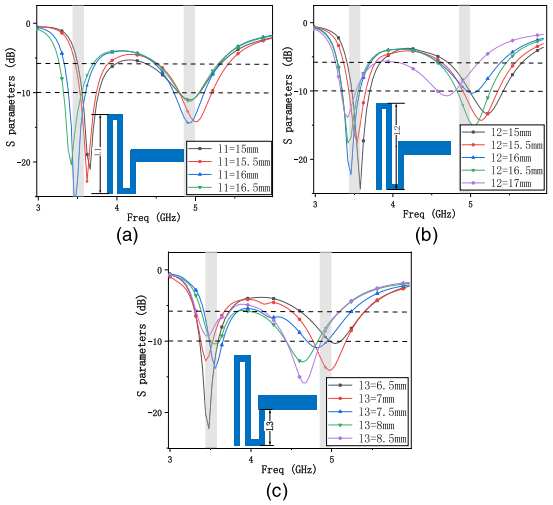

FIGURE 14. Simulate S-parameters of Ant 3 in 5G module with different values of (a) L1, (b) L2, (c) L3.

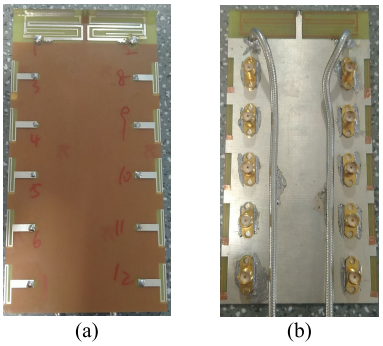

FIGURE 15. Photos of the manufactured MIMO antenna: (a)Top view, (b) Back view.

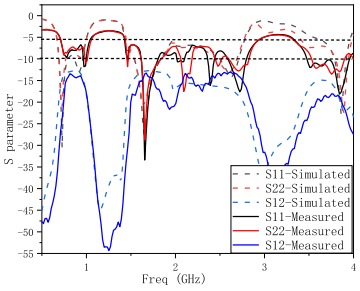

FIGURE 16. Measured and simulated S-parameters of the proposed 4G module antennas.

by the medium branch and the shortest branch. Band I and band II can be easily adjusted by tuning L1, L2, and L3.

IV. RESULTS AND DISCUSSION

The proposed twelve-port MIMO antennas system was fabricated, and its photos taken from the top and back views are presented in Fig. 15(a) and (b), respectively. The measured results were obtained in a microwave anechoic chamber using a vector network analyzer.

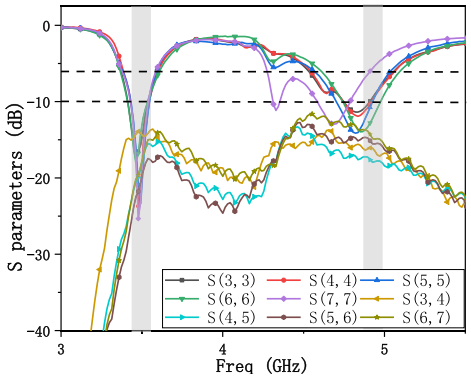

FIGURE 17. Measured S-parameters of the proposed 5G module antennas.

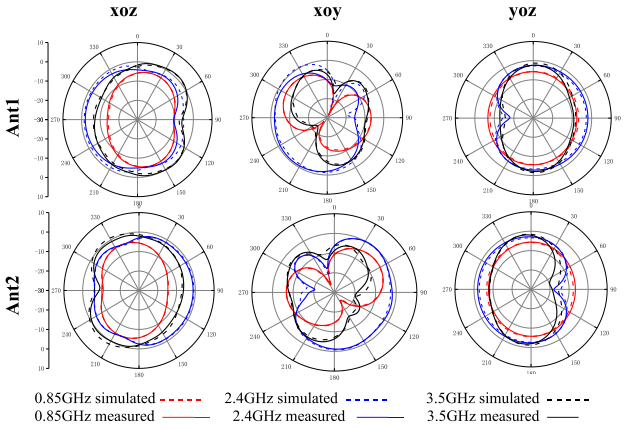

FIGURE 18. Radiation patterns for Ant1 and Ant 2 at different frequencies.

A. S-PARAMETERS

A comparison of the simulated and measured S-parameters of the proposed 4G module antenna is shown in Fig. 16. As shown in Fig. 16, the measured S_{11} and S_{21} values are lower than -6 dB and -12.5 dB, respectively, over 720-1025 MHz, 1445-2890 MHz, and 3370-4000 MHz, and agree well with the simulated data. Fig. 17 shows the measured S-parameters of the 5G module antennas. As can be seen in the figure, the operating bands of the 5G antenna module with S_{11} lower than -6 dB range over 3.37 $\sim$ 3.60 GHz and 4.50 $\sim$ 5.10 GHz, covering the 3.5-GHz band (3.4$\sim$3.6 GHz) and 4.9-GHz band (4.8 $\sim$ 5.0 GHz) for future 5G applications, and the measured isolation between the adjacent elements was better than 12.7 dB within the entire operating band.

B. RADIATION PERFORMANCES

Fig. 18 shows the measured and simulated radiation characteristics of the proposed 4G antenna system, which are in good agreement. It is worth noting that some complementary characteristics for Ant 1 and Ant 2 are presented at the same frequency. The result indicated that the 4G antenna module had a good pattern diversity ability to combat

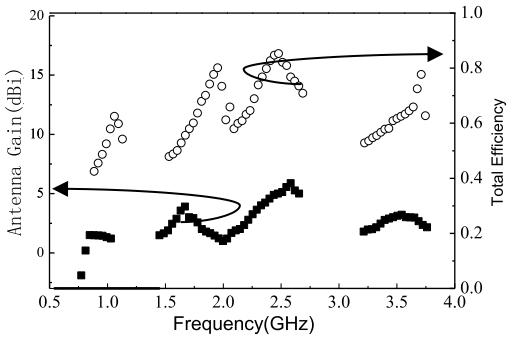

FIGURE 19. Measured antenna gain and total efficiency of the proposed 4G module antenna system.

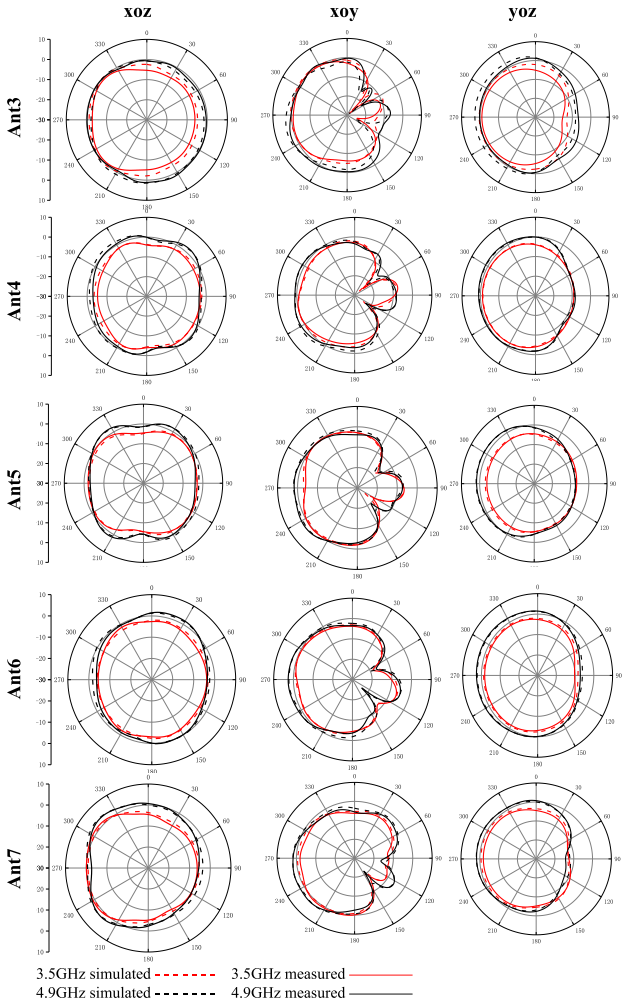

FIGURE 20. Radiation patterns for Ant3 to Ant7 at different frequencies.

multipath fading. The antenna gain and antenna total efficiency of the 4G antenna module were measured, and the results are shown in Fig. 19. The measured antenna gain varies from −1.9 to 1.52 dBi at the lower operating band, from 1.01 to 5.87 dBi at the middle band, and from 1.79 to 3.22 dBi at the higher band. The measured total efficiency is about 42.5%-62.5% at the lower band, about 47.9%-85.3%

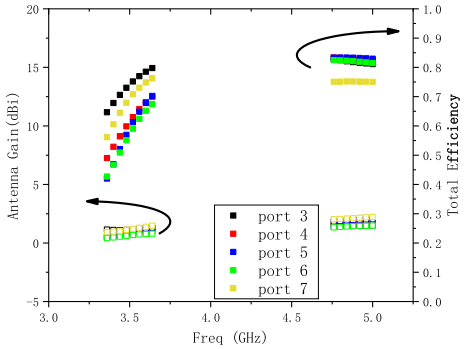

FIGURE 21. Measured antenna gain and total efficiency of the proposed 5G module antenna system.

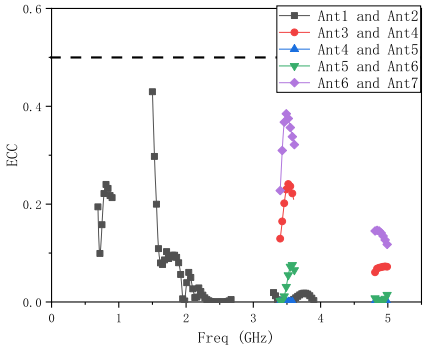

FIGURE 22. Calculated ECC of the proposed Twelve-port MIMO Antenna System.

at the middle operating band, and about 52.8%-77.7% at the higher band.

Fig. 20 shows the measured and simulated radiation characteristics of the proposed 5G module antenna system. The results of Ant 8–Ant 12 are omitted here, because their radiation patterns are almost the mirror images of Ant 3–Ant 7. In the three main planes, each 5G antenna element on the same side has shown similar radiation characteristics. The antenna gain and total efficiency of the 5G module antenna system were measured, and the results are presented in Fig. 21. The measured antenna gain results range from 0.41 to 1.48 dBi at the lower operating band, and from 1.33 to 2.23 dBi at the higher band. The measured total efficiency is about 42.5%-79.5% at the lower band, and about 75.1%-83.3% at the higher band.

C. MIMO PERFORMANCES

In order to illustrate the diversity performance of the MIMO antenna system, the envelope correlation coefficient (ECC) is usually evaluated. Generally, the MIMO antenna system shows a promising diversity when the value of ECC is less than 0.5. The envelope correlation coefficient between antenna a and antenna b, ρ_{ab}, can be calculated by [16]-[18]:

$$\rho_{ab} = \frac{\left|S_{aa}^{*}S_{ab} + S_{ab}^{*}S_{bb}\right|^{2}}{(1-|S_{aa}|^{2}+|S_{ba}|^{2})(1-|S_{bb}|^{2}+|S_{ab}|^{2})\eta_a\eta_b} \quad (4)$$

TABLE 1. Comparison between the proposed antenna and the referenced antennas.

	No. of ports	module	Operating bands (MHz)	Isolation (dB)	Efficiency (%)
Ref. [10]	10	4G	824-960	-11.25	≥40(LB)
			1710-2690		≥60(HB)
		5G	3400-3600	-10	62-78
Ref. [11]	8	5G	3400-3600	-17.5	62-76
Ref. [12]	8	5G	3400-3600	-11.2	51-59(LB)
			5150-5925		62-80(HB)
Ref. [13]	10	5G	3400-3800	-10	42-65(LB)
			5150-5925		62-82(HB)
Ref. [14]	8	5G	3400-4200	-12.5	53.8-76.5(LB)
			4800-5000		62.6-79.1(HB)
Ref. [15]	8	5G	3400-3600	-11.5	41-72 (LB)
			4800-5100		40-85 (HB)
Proposed antenna	12	4G	691-970	-11	42.5-6.25(LB)
			1430-2740		47.9-83.3(MB)
			3360-3960		52.8-77.7(HB)
		5G	3310-3700	-12.5	42.5-79.5(LB)
			4300-5180		81.1-83.3(HB)

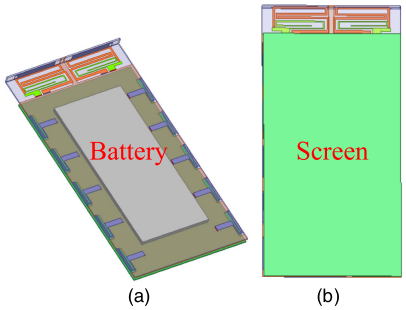

FIGURE 23. Simulated model of the proposed antenna with a battery and screen: (a) top view, (b) bottom view.

where S_{aa}, S_{ab}, and S_{bb} are the measured S-parameters of antenna a and antenna b; η_a and η_b denote the radiation efficiency of antenna a and antenna b, respectively.

Fig. 22 shows the calculated ECC of the proposed twelve-port MIMO antenna system. The values of the 4G antenna module are less than 0.42 and the values of the 5G antenna module are less than 0.4, over their operating bands. As the calculated ECCs are all better than the acceptable criterion of lower than 0.5, a desirable diversity capability is achieved by the proposed MIMO antenna.

D. EFFECT OF SCREEN AND BATTERY

In order to assess the performance of the proposed antenna in a real application, the screen and battery were added to the antenna system. Fig. 23 presents the simulation model of the proposed antenna with a battery and screen. As can be seen in Fig. 23, the battery was modeled as a copper block with a size of $95 \times 41 \times 2.5\ mm^3$ and the screen was modeled as a glass material with a size of $125 \times 70 \times 1mm^3$. As can be observed from Fig.24, the battery and screen have little effect on the frequency band of the 4G antenna module. Although a slight frequency shifting can be observed in the 5G antenna module, the S-parameters of the 5G antenna module still meet the needs in the two bands. In addition, the frequency

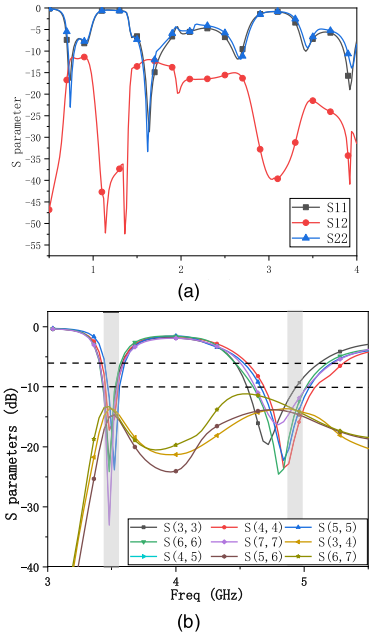

FIGURE 24. Simulated S-parameters of the proposed antenna with a battery and screen: (a) 4G module antennas (b) 5G module antennas.

bands of 5G antennas can be adjusted to the desired ones by tuning the length of branches. We also compared the total efficiency of the antenna with and without a battery and screen. The total efficiency of the 4G antenna is decreased by 1.8%-2.5%, while that of the 5G antenna decreased by 2.2%-4.6%. Nonetheless, the performance of the proposed antenna still meets the needs of 4G/5G smartphone applications.

Table 1 presents the comparison of the proposed antenna and the referenced antennas. It can be observed that the proposed antenna can work at more operating bands and cover more applications compared with the referenced antennas. The proposed antenna consists of a 4G and 5G antenna module, while most of the referenced antennas can only work in

5G applications. In addition, the proposed antenna has more ports and achieves good isolation. Furthermore, the proposed antenna has higher total efficiencies.

V. CONCLUSION

A twelve-port MIMO antenna system for multi-mode 4G/5G smartphone applications has been presented and investigated in this paper. The characteristic mode analysis (CMA) has been used to find potential resonance and explain the operating principle of the antenna. The 4G antenna array covers the bands of LTE700/2500/3400, GSM850/900, DCS, PCS, UTMS, 2.4-GHz WLAN and 3.5-GHz WiMAX successfully and achieves mutual coupling lower than −11 dB in the lower band and −15 dB in the upper bands by using the protruded ground between the two closely spaced antenna elements. The 5G antenna module is a 10 × 10 MIMO antenna array capable of covering the 3.5-GHz band (3.4 ∼ 3.6 GHz) and 4.9-GHz band (4.8 ∼ 5.0 GHz) for 5G applications. The measured results of S-parameters, radiation patterns, antenna gain, and antenna efficiency are presented and agree well with the simulated results. The envelope correlation coefficient (ECC) was calculated, and the values were lower than 0.5 and could meet the requirement of the MIMO antenna system. Hence, the proposed antenna is suitable for multi-mode 4G/5G smartphone applications.

REFERENCES

[1] D. Gesbert, M. Shafi, and D. S. Shiu, "From theory to practice: An overview of MIMO space-time coded wireless systems," *IEEE J. Sel. Areas Commun.*, vol. 21, no. 3, pp. 281–302, Apr. 2003.

[2] Z. Li, Z. Du, M. Takahashi, K. Saito, and K. Ito, "Reducing mutual coupling of MIMO antennas with parasitic elements for mobile terminals," *IEEE Trans. Antennas Propag.*, vol. 60, no. 2, pp. 473–481, Feb. 2012.

[3] M. Ikram, M. S. Sharawi, A. Shamim, and A. Sebak, "A multiband dual-standard MIMO antenna system based on monopoles (4G) and connected slots (5G) for future smart phones," *Microw. Opt. Technol. Lett.*, vol. 60, no. 6, pp. 1468–1476, Jun. 2018.

[4] Q. Sun, B. Sun, L. Sun, W. Huang, and Q. Ren, "Broadband two-element array with hybrid decoupling structures for multimode mobile terminals," *IEEE Antennas Wireless Propag. Lett.*, vol. 14, pp. 1431–1434, 2015.

[5] S. Wang and Z. Du, "A dual-antenna system for LTE/WWAN/WLAN/WiMAX smartphone applications," *IEEE Antennas Wireless Propag. Lett.*, vol. 14, pp. 1443–1446, 2015.

[6] J. Dong, X. Yu, and L. Deng, "A decoupled multiband dual-antenna system for WWAN/LTE smartphone applications," *IEEE Antennas Wireless Propag. Lett.*, vol. 16, pp. 1528–1532, 2017.

[7] Z. An and M. He, "A Multiband Dual-Antenna System for MIMO Operation in Mobile Terminals," *Appl. Comput. Electromagn. Soc. J.*, vol. 34, no. 10, pp. 1529–1534, Oct. 2019.

[8] K. Yu, Y. Li, and X. Liu, "Mutual coupling reduction of a MIMO antenna array using 3D novel meta material structures," *Appl. Comput. Electromagn. Soc. J.*, vol. 33, no. 7, pp. 758–763, 2018.

[9] M.-Y. Li, Y.-L. Ban, Z.-Q. Xu, J. Guo, and Z.-F. Yu, "Tri-polarized 12-antenna MIMO array for future 5G smartphone applications," *IEEE Access*, vol. 6, pp. 6160–6170, 2018.

[10] Y.-L. Ban, C. Li, C.-Y.-D. Sim, G. Wu, and K.-L. Wong, "4G/5G multiple antennas for future multi-mode smartphone applications," *IEEE Access*, vol. 4, pp. 2981–2988, 2016.

[11] Y. Li, C. Y. D. Sim, Y. Luo, and G. Yang, "High-isolation 3.5 GHz eight antenna MIMO array using balanced open-slot antenna element for 5G smartphones," *IEEE Trans. Antennas Propag.*, vol. 67, no. 6, pp. 3820–3830, Jun. 2019.

[12] J. Li, X. Zhang, Z. Wang, X. Chen, J. Chen, Y. Li, and A. Zhang, "Dual-band eight-antenna array design for MIMO applications in 5G mobile terminals," *IEEE Access*, vol. 7, pp. 71636–71644, 2019.

[13] Y. Li, C.-Y.-D. Sim, Y. Luo, and G. Yang, "Multiband 10-antenna array for Sub-6 GHz MIMO applications in 5-G smartphones," *IEEE Access*, vol. 6, pp. 28041–28053, 2018.

[14] L. Cui, J. Guo, Y. Liu, and C.-Y.-D. Sim, "An 8-Element dual-band MIMO antenna with decoupling stub for 5G smartphone applications," *IEEE Antennas Wireless Propag. Lett.*, vol. 18, no. 10, pp. 2095–2099, Oct. 2019.

[15] J. Guo, L. Cui, C. Li, and B. Sun, "Side-edge frame printed eight-port dual-band antenna array for 5G smartphone applications," *IEEE Trans. Antennas Propag.*, vol. 66, no. 12, pp. 7412–7417, Dec. 2018.

[16] S. Blanch, J. Romeu, and I. Corbella, "Exact representation of antenna system diversity performance from input parameter description," *Electron. Lett.*, vol. 39, no. 9, pp. 705–707, 2003.

[17] N. Kumar and R. Khanna, "A compact multi–band multi–input multi–output antenna for 4G/5G and IoT devices using theory of characteristic modes," *Int. J. RF Microw. Comput.-Aided Eng.*, vol. 30, no. 1, Jan. 2020, Art. no. e22012.

[18] P. Hallbjorner, "The significance of radiation efficiencies when using S-parameters to calculate the received signal correlation from two antennas," *IEEE Antennas Wireless Propag. Lett.*, vol. 4, pp. 97–99, 2005.

JIAN DONG received the B.S. degree in electrical engineering from Hunan University, Changsha, China, in 2004, and the Ph.D. degree in electrical engineering from the Huazhong University of Science and Technology (HUST), Wuhan, China, in 2010. From 2006 to 2010, he was a Research Assistant with the National Key Laboratory of Science and Technology on Multispectral Information Processing, HUST. From 2012 to 2019, he was an Associate Professor with the School of Information Science and Engineering, Central South University, Changsha. From 2016 to 2017, he was a Visiting Scholar with the Eledia Research Center, University of Trento, Italy. He is currently a Full Professor with the School of Computer Science and Engineering, Central South University. He has published six books and over 100 peer reviewed articles on international journals and conferences. He holds over 16 innovation patents. His current research interests include antennas, wireless communications, and numerical optimization techniques.

SHAN WANG received the B.S. degree in communication engineering from Central South University, Changsha, China, in 2018, where she is currently pursuing the M.S. degree. Her current research interests include multiple-input multiple-output antennas and multiband antennas.

JINJUN MO received the B.S., M.S., and Ph.D. degrees in electrical engineering from the National University of Defense Technology (NUDT), Changsha, China, in 1997, 2000, and 2004, respectively. From 2004 to 2008, he was a Lecturer with the College of Electronic Science and Engineering, NUDT. He was an Associate Professor, from 2009 to 2017. From 2011 to 2012, he was a Visiting Scholar with the Poly-Grames Research Center, University of Montreal, Canada. From 2018 to 2019, he was a Special-Term Professor with the School of Aeronautics and Astronautics, Central South University, Changsha. Since November 2019, he has been with the School of Information and Communication, Guilin University of Electronic Technology, Guilin, China, as a Professor. He has published five books and over 40 peer reviewed articles on international journals and conferences. His current research interests include antennas, computational electromagnetics, and numerical optimization techniques.